EFDA–JET–PR(06)21

G. Saibene, N. Oyama, J. Lönnroth, Y. Andrew, E. de la Luna, C. Giroud,
G.T.A. Huysmans, Y. Kamada, M.A.H. Kempenaars, A. Loarte, D.McDonald,
M.M.F Nave, A. Meiggs, V. Parail, R. Sartori, S. Sharapov, J. Stober,
T. Suzuki, M Takechi, K Toi, H Urano and JET EFDA contributors

The H-Mode Pedestal, ELMs and TF Ripple Effects in JT-60U/ JET Dimensionless Identity Experiments

The H-Mode Pedestal, ELMs and TF Ripple Effects in JT-60U/ JET Dimensionless Identity Experiments

G. Saibene[1], N. Oyama[2], J. Lönnroth[3], Y. Andrew[4], E. de la Luna[5], C. Giroud[4], G.T.A Huysmans[6], Y. Kamada[2], M.A.H Kempenaars[7], A. Loarte[1], D. McDonald[3], M.M.F. Nave[8], A. Meiggs[4], V. Parail[4], R. Sartori[1], S. Sharapov[4], J. Stober[9], T. Suzuki[2], M. Takechi[2], K. Toi[10], H. Urano[2] and JET EFDA contributors*

[1]EFDA Close Support Unit - Garching, 2 Boltzmannstrasse, 85748 Garching, Germany
[2]Fusion Research and Development Directorate, JAEA, Naka, Ibaraki, Japan
[3]Association Euratom-Tekes, Helsinki University of Technology, Finland
[4]Euratom/UKAEA Fusion Association , Culham Science Centre, Abingdon OX14 3EA, UK
[5]CIEMAT-Euratom Association, Av Complutense 22, E28040 Madrid, Spain
[6]Association Euratom/CEA, F13108 Cadarache, St. Paul-lez-Durance, France
[7]FOM-Rijnhuizen, Association Euratom-FOM, TEC, PO Box 1207, Nieuwegein, The Netherlands
[8]Centro de Fusao Nuclear, Euratom-IST Association, Av Rovisco Pais, Lisbon, Portugal
[9]Association Euratom/IPP, Max Plank Institüt für Plasmaphysik, 2 Boltzmannstrasse, 85748 Garching, Germany
[10]National Institute for Fusion Science, Gifu, Japan
** See annex of M.L. Watkins et al, "Overview of JET Results ",*
(Proc. 21st IAEA Fusion Energy Conference, Chengdu, China (2006)).

Preprint of Paper to be submitted for publication in
Nuclear Fusion

ABSTRACT.

This paper summarises results of dimensionless identity experiments in JT-60U and JET, aimed at the comparison of the H-mode pedestal and ELM behaviour in the two devices. Given their similar size, dimensionless matched plasmas are also similar in their dimensional parameters (in particular the plasma minor radius a is the same in JET and JT-60U). Power and density scans were carried out at two values of I_p, providing a q scan (q_{95} = 3.1 and 5.1) with fixed (and matched) toroidal field. Contrary to initial expectations, a dimensionless match between the two devices was quite difficult to achieve. In general, p_{ped} in JT-60U is lower than in JET and, at low q, the pedestal pressure of JT-60U with a Type I ELMy edge is matched in JET only in the Type III ELM regime. At q_{95} = 5.1, a dimensionless match in $\rho*$, $\nu*$ and $\beta_{p,ped}$ is obtained with Type I ELMs, but only with low-power JET H-modes. These results motivated a closer investigation of experimental conditions in the two devices, to identify possible "hidden" physics that prevents obtaining a good match of pedestal values over a large range of plasmas parameters. Ripple-induced ion losses of the medium bore plasma used in JT-60U for the similarity experiments are identified as the main difference with JET. The magnitude of the JT-60U ripple losses is sufficient to induce counter-toroidal rotation in co-injected plasma. The influence of ripple losses was demonstrated at q_{95} = 5.1: reducing ripple losses by $\approx$ 2 (from 4.3 to 1.9MW) by replacing Positive with Negative Neutral Beam injection at approximately constant P_{in}, resulted in an increased p_{ped} in JT-60U, providing a good match to full power JET H-modes. At the same time, the counter-toroidal rotation decreased. Physics mechanisms relating ripple losses to pedestal performance are not yet identified, and the possible role of velocity shear in the pedestal stability, as well as the possible influence of ripple on thermal ion transport are briefly discussed. Toroidal rotation of the ITER reference inductive Q = 10 H-mode is predicted to be rather low, of the order of ~1/10 of the frequency of typical JET H-modes. Nonetheless, fast ion ripple losses in that scenario are also predicted to be negligible (<1%), and therefore plasma toroidal rotation slow-down or ripple-induced counter-rotation should not affect pedestal parameters and stability in ITER. Finally, the possible effect of ripple on thermal transport may deserve more attention in future experiments and modelling, since the ripple magnitude of ITER is intermediate between that of JET and JT-60U.

1. INTRODUCTION

This paper describes the results of dimensionless identity experiments in JT-60U and JET, aimed at the comparison of the plasma pedestal characteristics and ELM behaviour in the two devices. The method chosen for this study is the "dimensionless identity technique", based on the invariance of plasma physics to changes of dimensional parameters (n_e, T_e at the pedestal, for instance), when the dimensionless plasma parameters are conserved: safety factor $q \propto B_T a^2/RI_p$, normalized plasma pressure $\beta \propto n_T/B^2_T$ (assuming $T_e = T_i$ and $n_e = n_i$), Larmor radius $\rho^* \propto T^{1/2}/B_T a$ and e–e (e = electron) neoclassical collisionality $\nu^* \propto Rq\varepsilon^{-3/2} n/T^2$. A simultaneous match of the four parameters above leads to the following scaling for the plasma current I_p, toroidal field B_T, density n and

temperature T : $I_p \propto R^{-3/8}a^{1/8}$, $B_T \propto R^{5/8}\, a^{-15}$, $n \propto a^{-2}$ and $T \propto R^{5/4}\, a^{-7/4}$, $n \propto a^{-2}$. In contrast to other dimensionless comparison experiments, the similar size of JET and JT-60U results in dimensionless matched plasmas that are also almost identical in their dimensional parameters, with the exception of the major radius R. Moreover, the fact that the plasmas dimensions in the two devices are so similar means that matching q_{95} results in a very close match of the edge poloidal fields in the two devices (within 5%).

The main geometrical parameters of the equilibria used in the experiments are listed in table 1, illustrating the good match achieved in the equilibria in the two devices, with the exception of the inverse aspect ratios ε which differ, for the particular discharge geometry required by the experiments, by ≈ 15% ($\varepsilon_{JET} = 1.16\, \varepsilon_{JT\text{-}60U}$). The verification of dimensionless scalings in such highly constrained conditions (H-mode threshold power P_{th}, plasmas stored energy W_p, ELM frequency f_{ELM}, etc. should be very near in value) provides an excellent test-bed for the scaling hypothesis and for identifying additional physics phenomena that can affect extrapolations of present data to future devices.

The paper is organised as follows: section 2 contains a short description of experimental conditions and plasma parameters explored in the two devices for the similarity studies. All experimental results are grouped in section 3. Scalar pedestal parameters are described and compared in sub-sections 3.1 and 3.2, while sub-section 3.3 compares ELM behaviour in JET and JT-60U plasmas, as well as briefly discussing global confinement. The analysis of pedestal and core profiles for selected pairs of plasma discharges is presented in 3.4. Sections 4 and 5 discuss the results, including possible implications for ITER.

2. THE EXPERIMENTS

As described in [13], a special "JT-60U-like" equilibrium was developed in JET to match the magnetic geometry of the diagnostic optimised, medium bore plasma used in JT-60U for H-mode pedestal studies.

This particular configuration in JT-60U, shifted to the low-field side of the device to optimise the line of sight of edge profile diagnostics, is characterized by relatively high value of the toroidal field ripple in the separatrix region (≈ 1.2%), causing fast particle losses and limiting the net available input power to the plasma. The plasma minor radius a is the same in the two devices, and geometric quantities such as elongation κ and triangularity δ are matched within $\lesssim$2% ($\kappa \approx 1.46$, $\delta \approx 0.27$). The dimensionless identity comparison was focussed on two matching combinations of I_p and B_T. The first was a plasma with 1.8MA/3.17T in JT-60U matching 1.9MA/2.9T in JET with $q_{95} = 3.1$, while the second was a 1.08MA/3.17T discharge in JT-60U, corresponding to 1.15MA/2.9T for JET, and $q_{95} = 5.1$. This combination of plasma parameters provides a q_{95} variation at constant B_T.

The experiments described in this paper complement and extend those described in an early publication ([13]), by including new data for the high current/low *q* plasmas , as well as low current/ higher q_{95} experimental results, not available at the time of the earlier publication.

The additional heating scheme in JT-60U was Positive Neutral Beam injection (PNB) or a combination of P NB and negative-ion neutral beam injection (NNB, at ≈ 360kV , co-injection). In the JET experiments, most plasmas were P NB heated, while a few had PNB and ICRH (Ion Cyclotron Resonance Heating) hydrogen minority combined heating. While the injection energy of the P NB systems in JET and JT-60U is similar (80 and 105keV in JET versus 85keV in JT-60U), the injection geometry is not. Most of the P NB input power in JT-60U is provided by perpendicular injection (up to ~ 14MW), with further 4.4MW each available from co-injection and counter-injection sources. In the experiments described in this paper, the JT-60U beam sources were always combined to provide net co-injection In contrast, all the sources in JET are in co-injection, up to maximum input power of ≈ 20MW. Given the differences in the neutral beam systems in the two devices, the injected torque is higher in JET than in JT-60, for the same input power, although the torque per MW will depend on the exact beam mix used in both machines. For instance, for ~10MW P_{in}, the torque injection in these JT-60U experiments was typically between ~ 6 and ~8Nm, while in JET this is of the order of 15Nm. A detailed description of the neutral beam system in JT-60U is found in [Kuriyama et al., 2002], while the JET system is described in [Challis and the JET Team, 1995].

During the experiments, input power and fuelling were varied to scan a range of edge densities and temperature, obtaining an overall variation of ν^* at the pedestal between ≈ 0.02 and 1, and of ρ^* from ≈ 2×10^{-3} to 4.5×10^{-3}. The net input power P_{in} was between 4–10MW (JET) and 6–10MW (JT-60U) at low current, while varied between 7 and 14MW (JET) and 10-13.5MW (JT-60U) at high current. The majority of discharges at both currents had a Type I ELM edge, but data in the Type III ELMy regime were also obtained, in both devices.

As mentioned at the beginning of this section, one major difference between JET and JT-60U is the Toroidal Field (TF) coils number and geometry, leading to large differences in the toroidal field ripple in the two devices. Specifically, JET is equipped with 32 D-shaped coils, while JT-60U has 18 quasi-circular T F coils. A map of the ripple amplitude for JET, with the plasma equilibrium used for these experiments is shown in figure 2, and in figure 3 for JT-60U with the JET similarity equilibrium.

The two figures show that, for the particular equilibria used in the experiments, the ripple intensity for JET is ≈ 0.1% at the outer midplane separatrix position, while for JT-60U this is ≈ 1.2%. While the JET ripple is essentially negligible, the ripple intensity in JET similarity JT-60U plasmas is large enough (combined with the predominant perpendicular direction of the NB injection) to cause large fast ion losses, up to 40–50% of the net injected power, for positive beam injection. This is discussed in more details in section 3.1.

The attention given in this paper to the toroidal filed ripple and its effects is partly based on the results of the first JT-60U/JET similarity experiments, reported in [13], describing the results of an initial set of similarity discharges at low q_{95} and PNB injection. That analysis showed that the major difference between JET and JT-60U plasmas was in the plasma toroidal rotation, associated to ripple-induced fast ion losses in JT-60U (see section 3). As a consequence of that analysis, of the

main aims of the experiments reported in this work was to study the role of ripple losses and rotation on the H-mode pedestal and H-mode performance. the time of the earlier publication.

3. RESULTS

3.1 COMPARISON OF PEDESTAL PARAMETERS

A first comparison of plasma characteristics in JET and JT-60U is obtained by studying the behaviour of the pedestal density and temperatures for varying input power and gas fuelling. The dimensional comparison is based on the analysis of pedestal top electron density and temperature, while the dimensionless analysis (section 3.2) also requires ion temperature data (T_i). For JET, ne is measured with a FIR interferometer, while T_e is obtained from ECE; T_i at the pedestal top is measured by charge-exchange recombination spectroscopy, (more details in [15]). For JT-60U, n_e and T_e are measured with a Thomson Scattering system, while T_i is obtained from charge-exchange measurements, as in JET. Typical error bars for these measurements are shown in the figures of the relevant profiles in section 3.4.

The value of electron density ($n_{e,ped}$) and temperature ($T_{e,ped}$) at the top of the pedestal are compared in figures 4 and 5, for all discharges with q_{95} of 3.1 and 5.1 respectively.

The two figures show immediately that the pedestal electron pressure ($p_{e,ped}$) of JT-60U plasmas tends to be lower than that of equivalent JET discharges, by up to a factor of two for PNB plasmas. This is particularly evident for the higher I_p experiments (figure 4), where the range of pedestal n_e–T_e obtained in JT-60U with Type I ELMs is accessible in JET only if the plasma is deliberately driven to Type III ELMs. This is not the case for the low I_p, high q_{95} set of discharges (figure 5): similar pedestal pressure for JET and JT-60U H-modes could be obtained by reducing the input power in JET (either PNB or PNB+ICRH) to levels near or slightly below the empirical average minimum input power required to maintain a steady state Type I ELMy H-mode in JET (at this triangularity $P_{in}/P_{Th} \gtrsim 2$ [16], with P_{th} being the H-mode threshold power as defined in [3]). It is observed that at low power ($P_{in}/P_{Th} \lesssim 1.8$) and at low densities ($n/n_{GR} \lesssim 50\%$), compared to typical JET ELMy H-mode operation, Type I ELMy H-modes can be sustained although the pedestal is not “fully developed”. In fact, in these conditions, p_{ped} increases with P_{in}, although this dependence saturates at higher input powers. This power dependence of p_{ped} is not observed for the JT-60U H-modes analysed in this paper, consistently with results from earlier analysis of low δ H-mode pedestals in JT-60U [21].

The pedestal behaviour of these JET similarity ELMy H-mode was successfully exploited to “drive” the JET pedestal parameters towards the values observed in JT-60U, resulting in the Type I ELMs points with $n_{e,ped}$ ~ 1.4 to 2.0×10^{19} m^{-3} and $T_{e,ped}$ between 0.8 and 1.3keV, very near to typical Type I ELMy H-mode pedestal parameters of JT-60U similarity discharges. The marginality for Type I ELM pedestals in JET at these low input power is demonstrated by the coexistence at very similar pedestal parameters of Type I ELMy H-modes with plasmas at the transition between Type III and Type I regimes (black squares with a cross, figure 5).

As mentioned in section 2, the medium bore plasmas required in JT-60U for the identity experiments with JET suffer from large BT ripple-induced fast ion losses. In particular, the ripple perturbation at the low fieldside of the JET identity plasmas in JT-60 reaches ~ 1.2% (figure 3), to be compared with ~ 0.1% in JET. For the plasma configuration used in these experiments, the typical JT-60U fast ion ripple losses are of the order of ~ 40% of P_{in} (for PNB) both at high and low I_p. The evaluation of these losses for the JT-60U experiments is routinely carried out using the OFMC code [19]. The typical uncertainty in the calculations of fast ion losses (including statistical error and plasma profile uncertainties) is $\lesssim 5\%$.

Apart from limiting the total amount of net input power to the plasma, previous studies on JT-60U plasmas showed that ripple-induced fast ion losses can produce a toroidal counter-rotation source in the plasma edge ([20], [6]). More recently, [22] reported on a series of dedicated experiments in JT-60U for the study of the effect of ripple and toroidal rotation on pedestal parameters, showing that plasma counter-rotation increases with the magnitude of the BT ripple, at constant momentum input by the beams. Ripple-induced counter toroidal rotation was observed in all similarity plasmas studied here (figure 6, full symbols): all plasmas with PNB injection rotate in the counter-current direction, in spite of positive (i.e. co-current) net momentum injection provided by the beams. This is a clear difference with the JET experiments (figure 6, full squares), where plasmas are always co-rotating for beam co-injection.

The possible effects of rotation and ripple losses on the pedestal were addressed experimentally in JET similarity discharges in JT-60U. Ripple-induced fast ion losses were reduced by changing the beam make-up: most PNB perpendicular sources were substituted by NNB, reducing the fast ion power losses by as much as 60%, while keeping the net input power approximately constant. Time traces of one of such a discharge are shown in figure 7, for pulse E43075, with $q_{95} = 5.1$. Most perpendicular PNB sources are substituted by ~ 4.5MW NNB at t = 7s, reducing the fast ion losses from ~ 4.3MW (at 5.5s) to ~ 1.8MW at 7.6s, at constant net power input of ~ 8.6MW (the perpendicular beam contribution is reduced from 9.1 down to 2.3MW). The net absorbed power increases later in the pulse to ~ 9MW (at 8.5s) due to an increase of the NNB injected power. The change in beam energy and injection geometry produce approximately a factor of 2 increase of the injected toroidal torque (positive direction, i.e. co-current). The reduction in fast ion losses corresponds to a change of the whole toroidal rotation profile; rotation at the plasma edge is reduced in magnitude, but does not change sign (figure 6).

A similar experiment was attempted in a low q_{95} JET similarity plasma in JT-60U. As for the case of the low q_{95} pulse, 4.3MW NNB were injected in pulse E43058 to substitute for part of the positive perpendicular neutral beam sources. For this and the other low q_{95} pulses with NNB, due to availability of the beam system, the perpendicular PNB were reduced only from ~ 9.0 to ~ 4.7MW , leading to a smaller change in fast ion losses, from 4.5 to 2.9MW or just ~ 35%. Moreover, the control of the net total power was not as good as for pulse E43075, with the net power being somewhat higher in the NNB than in the PNB phase (11.6 versus 10.7MW). Nonetheless, the

plasma rotation response is qualitatively similar to the high q_{95} case, as shown in figure 6. Specifically, figure 6 shows that the magnitude of the plasma response to the changes in fast ion losses is larger for the low I_p case, consistent with the larger reduction of fast ion losses achieved by changing the NB injection mix, compared to the plasmas with q_{95} = 3.1. On the other hand, the plasma toroidal rotation profiles of both high and low q plasmas in the phases with NNB are the same, at least for $\rho \gtrsim 0.5$.

The effect of changing fast ion losses (and rotation) on the pedestal parameters of the JT-60U similarity plasmas can be seen in figures 4 and 5, for the low and high q_{95} series of experiments respectively. The pedestal parameters during NNB phases are represented with green dots. At q_{95} = 5.1, a large increase in the pedestal parameters is correlated to NNB injection, achieving p_{ped} higher than any of those obtained with PNB. The increase in the pedestal pressure is mainly due to an increase of the pedestal temperature (both T_e and T_i, as shown in figure 7, for the example of pulse E43075), leading to ~ 50% improved pedestal pressure, compared to the average value of p_{ped} with PNB only. In contrast, only a very modest improvement in the pedestal parameters is observed for the pulses at low q_{95}, of ~ 15%, just outside the statistical variation of p_{ped} obtained with PNB.

As mentioned above, the magnitude of the variation of V_{Tor} profile correlates with the size of the reduction of fast ion losses. This is consistent with the idea that the fast ion losses are the primary drive for the counter-rotation.

3.2 DIMENSIONLESS PEDESTAL PARAMETERS

Figures 8 and 9 show the comparison of $\rho*$, $\nu*$ and $\beta_{p,ped}$ obtained in power/density scans for both q_{95} = 5.1 and q_{95} = 3.1 series of experiments. The plots include P NB and NNB heated plasmas in JT-60U and, for JET, PNB and PNB + ICRH H-modes (these are not distinguished in the graphs since the pedestal parameters obtained did not change with the heating mix). All dimensionless parameters are calculated at the pedestal top, and $\beta_{p,ped} = 2\mu_0 p_{ped,tot} / \langle B_p \rangle_V^2$, i.e. $\beta_{p,ped}$ is the total pedestal pressure ($p_{ped,tot} = n_i T_i + n_e T_e$) normalized to the volume average poloidal field.

Figure 8(a) shows that the range of ρ^*_{tor} achieved in the two devices is similar, in particular if only Type I ELMy H-modes are considered. For $\rho^*_{tor} \sim 3\times10^{-3}$, JET and JT-60U pedestals have also similar ν^*_e (for both PNB and NNB). For PNB discharges, a simultaneous match of $\rho*_{tor}$, ν^*_e and $\beta_{p,ped}$ (q is fixed) between JET and JT-60U is found only at relatively low JET pedestal pressures. Specifically, the best dimensionless match between the two devices is obtained for the JT-60U H-mode E45065 (P_{in} ~ 8.8MW, P_{in}/P_{Th} ~ 2.5, using the scaling for Pth reported in [18]), matching the JET low power ELMy H-mode 60849 (P_{in} ~ 7.6MW , P_{in}/P_{Th} ~ 1.8). The dimensionless comparison confirms the picture obtained by a straight comparison of the pedestal parameters, that is that the pedestal of JET and JT-60U are relatively poorly matched, apart from the case when the JET H-modes are marginal for Type I ELMs access. Figure 8 also shows that the highest ≤p,ped H-modes in JET and JT-60U are obtained at completely different values of $\rho*_{tor}$.

A somewhat different picture emerges if the pedestal data are cast in a dimensionless form using

ρ^*_{pol} instead of ρ^*_{tor}. As highlighted in figure 8 (c), a match is now obtained in the $\rho^*_{pol} - \beta_{p,ped}$ space for the high $\beta_{p,ped}$ data obtained with NNB heating in JT-60U (example, pulse E43075, P_{in} ~ 8.6MW, P_{in}/P_{Th} ~ 2.5) and the JET ELMy H-mode at higher power, such as pulse 60856, P_{in} ~ 10MW and P_{in}/P_{Th} ~ 2.7. Interestingly, both JET and JT-60U report scaling of the H-mode pedestal width with ρ^*_{pol} (see [4] and [14]). The ν^* of the JET and JT-60U matching discharges are ~ 0.07 and ~ 0.13 respectively that, although this does not represent a perfect match it is reasonably near, also accounting for experimental uncertainties. In the $\rho^*_{pol} - \beta_{p,ped}$ dimensionless pedestal parameters representation, JET and JT-60U PNB data now do not match very well any longer, and the few points with comparable $\rho^*_{pol} - \beta_{p,ped}$ have ν^* differing by at least a factor of 3.

The data points from the experiments at $q_{95} = 3.1$ in the $\rho^*_{tor} - \nu^*$ and $\rho^*_{tor} - \beta_{p,ped}$ spaces are shown in figure 9 (a) and (b). Both figures show that the common parameters space between the two devices is reduced compared to the high q case, in particular if one restricts the comparison to Type I ELMy H-modes only. Nonetheless, the JET Pulse No: 59219 (P_{in} ~ 11.2MW , P_{in}/P_{Th} ~ 1.8 and gas fuelling to reduce Tped, black star in the figures) is a good match to both JT-60U pulse E43072 (PBN, P_{in} ~ 13MW and P_{in}/P_{Th} ~ 2.3) and pulse E43059 (PNB + NNB, P_{in} ~ 12MW and P_{in}/P_{Th} ~ 2.8). The match between JET and JT-60U data is much poorer as function of ρ^*_{pol}, in particular no match is found in terms of pedestal collisionality.

3.3 GLOBAL CONFINEMENT AND ELM LOSSES

Although dimensionless identical H-mode pedestals have been obtained in JET and JT-60U, the global plasma confinement in JT-60U is systematically lower than in JET, also for matching pedestal conditions. This is illustrated in figure 10 for both the $q_{95} = 3.1$ and $q_{95} = 5.1$ data sets. For the data set at the higher I_p (figure 10 (a)), the average H98 for the JT-60U pulses is ~ 0.8 while for JET , $\langle H_{98} \rangle$ ~ 1.07. The global thermal confinement of the JT-60U pulses is the same for PNB and NNB heated plasmas, as expected since the pedestal pressure of the JT-60U H-modes did not vary, at low q_{95} when changing the heating mix. Moreover, these data indicate that the change in toroidal rotation between PNB and NNB does not have an effect on global confinement. The overall picture is similar for the low I_p data set, where $\langle H_{98} \rangle_{JT-60U}$ ~0.85, to compare with ~1.1 for JET. It is interesting to note that the improved pedestal pressure with NNB injection does not translate in a similarly higher overall confinement of the plasma: inspection of the plasma profiles for the JT-60U pulse E43075 shows indeed that only the local pedestal value improve with NNB, while the core profiles (n_e, T_i and T_e) are very similar for both P NB and P NB + NNB phases of the discharge.
The low I_p data set spans a larger range of $\beta_{p,ped}$ than that at low q_{95} allowing the identification of different trends in the confinement behaviour in the two machines. Figure 10 (b) shows quite clearly that, in the case of JET data, the global energy confinement enhancement factor increases with pedestal pressure, while this is not the case for the JT-60U plasmas.

It is unlikely that the large difference in the average confinement enhancement factors can be attributed to the small difference in the aspect ratio between the two devices (~ 15%). The core

MHD activity is very similar in both JET and JT-60U, essentially dominated by sawteeth, and discharges with NTMs have been excluded from this analysis.

The behaviour of ELM frequency f_{ELM} (as function of the power crossing the separatrix, $P_{sep} = P_{in} - P_{rad,bulk} - dW/dt$) and ELM power losses (defined as $P_{ELM} = \langle \Delta W_{ELM} \rangle \times f_{ELM}$, with $\langle \Delta W_{ELM} \rangle$ = average energy loss per ELM) has also been analysed for these experiments. Figure 11 shows an overview of the variation of f_{ELM} as function of P_{sep} for both q_{95} in the two devices. The overall result is that ELM frequencies are generally quite different in the two machines, with JT-60U ELMs being more frequent than JET ELMs, for comparable P_{sep}. This is illustrated very clearly for the $q_{95} = 3.1$ experiments (figure 11 (a)): for the same P_{sep} and similar edge densities, f_{ELM} is higher in JT-60U then in JET by a factor $1.5 - 3$. The same is true for the lower I_p similarity discharges, although the picture is superficially less clear, due to the fact that gas fueling and power were changed in JET quite substantially to try to match the JT-60U ELM frequencies. Although the figure shows some JET and JT-60U points to the left of figure 11 (b) very near to each others, these discharges are a in reality a poor match in terms of pedestal parameters, because of the much higher pedestal density of the JET pulses, caused by the external gas fueling used to increase f_{ELM}. The same considerations apply to the analysis of the dimensionless ELM frequency f_{ELM}/ω_c ($\omega_{ce} = eB/m$): these were compared for the matching pairs of JET and JT-60U discharges identified above (see subsection 3.2). For all PNB injections cases, the dimensionless frequencies do not match, with f_{ELM}/ω_c(JT-60U) ~ 1.3–1.6 the JET values. In contrast, a good match of f_{ELM}/ω_c is found for the $q_{95} = 5.1$ NNB JT-60U discharges an their dimensionless matched pulse in JET, with f_{ELM}/ω_c for the matched pair differing by <10%.

The difference in ELM and pedestal characteristics between JET and JT-60U similarity discharges is perhaps highlighted most by the analysis of ELM power losses. In fact, the fraction of power carried by Type I ELMs (P_{ELM}/P_{sep}, see figure 12) is very different in the two devices, for all discharges, even for those with matched f_{ELM}. For both currents, P_{ELM} in JT-60U ELMy H-modes is at most 20% of the power crossing the separatrix, while for the JET discharges of these experiments, P_{ELM}/P_{sep} is ~ 60%. This shows directly that, for the same P_{sep}, inter-ELM transport in JT-60U is much higher than in JET, since the plasma energy content of JT-60U is the same or lower than in JET.

3.4 PLASMA PROFILE COMPARISON

The comparison of the pedestal (and core) profiles of dimensionless matched JET and JT-60U H-modes may help to gain further insight in the underlying physics mechanisms determining the similarities and difference in the H-mode characteristics of the two devices. This section deals first with the profile analysis of the $q_{95} = 5.1$ similarity discharges, both for P NB and NNB heating, and then the lower q are discussed. The analysis of the profiles is carried out for the pairs of shots that achieved the best match in terms of pedestal top dimensionless parameters (see subsection 3.2, and the figures therein). For the pedestal, the profile analysis concentrates on electron temperature and

density profiles, since the quality of the JET pedestal ion temperature profiles was not sufficient for a meaningful comparison with JT-60U. While all the data from JT-60U are obtained using a high resolution Thomson scattering diagnostic, in JET the T_e profile data are obtained by a combination of ECE and edge LIDAR profiles (the latter providing high space resolution data, but limited in most cases to the gradient region of the pedestal). The n_e profiles for JET are obtained from edge and core LIDAR measurements, and in most cases supplemented by a single point density measurement from a vertical interferometer chord measuring in the pedestal top region.

Figure 13 shows a comparison of electron temperature and density profiles for two matching discharges at q_{95} = 5.1, for the case when PNB only was used in JT-60U. Specifically, figure 13 (a) compares T_e profiles for the pair E43065 (JT-60U, P NB) and JET Pulse No: 60849, while figure 13 (b) shows ne profiles for the same pair of shots. Likewise, figures 14 (a) and (b) show the same data, for a pair of matching discharges where the JT-60U plasma was with NNB injection (JT-60U E43075 at 7.6s, matching the JET Pulse No: 60856). The scaled JET $T_e(r)$ ($T \propto R^{5/4}a^{7/4}$ but $a_{JET} = a_{JT-60U}$) is also shown for easy comparison of the data from the two devices; for density, $n \propto a^2$, meaning that the scaled profiles are the same as the actual ones. The data for both pairs show that when the T_e pedestal top values are matched, a reasonable match is obtained across the profiles, both in width and gradients, although the JET plasmas reach a somewhat higher T_e than expected from the dimensionless scaling. The picture is quite different for the pedestal densities. The profiles compared in figure 13 (b) are quite typical: the density pedestal of JET is much higher and wider than that of JT-60U, although the ratio between JET and JT-60U pedestal density height and width varies depending on the pair of discharges. A comparison of the edge density gradient ∇n_e is not straightforward for the discharges analysed here, since $n_e(r)$ of these JET discharges is measured with good space resolution only over a part of the pedestal density gradient region and the radial localisation of the FIR measurement is poor (~ 12cm). Nonetheless, the indication is that, in general, the pedestal density profiles in JET are steeper than in JT-60U (see also [13]). The profile data confirms the results of the scalar analysis, that showed that the main difference between JET and JT-60U pedestal is found in the achievable density.

The above considerations do not fully apply to the density profile of the q_{95} = 5.1 JT-60U NNB heated discharge E43075 (figure 14 (b)): in this case the pedestal densities obtained in JET and JT-60U are quite similar (within ~ 15%), consistently with the improved pedestal pressure obtained with NNB heating in JT-60U H-modes at high q_{95} (figure 5). Density gradients cannot be quantitatively compared, because in this case, the JET edge LIDAR settings were such that the measured gradient is limited by the instrument resolution.

The pedestal T_e and n_e profiles for the q = 3.1 experiments are compared in figure 15. As discussed in section 3.1, the behaviour of the pedestal of JT-60U H-modes (in terms of scalar pedestal top values) was very similar for PNB and PNB + NNB heated plasmas, probably due to the relatively small reduction of fast ion losses achieved in those experiments when changing the beam mixture. This is confirmed also from the profile analysis for discharges 59219 (JET) and E43072 (JT-60U,

PNB) and E43059 (JT-60U, PNB+NNB): a good match is obtained for the electron temperature profiles between the three plasmas while the density match is rather poor, similarly to what observed for the PNB matches at $q_{95} = 5.1$.

A comparison of the core profiles is quite complex, and would require a full transport analysis of the matching discharges, outside the scope of this paper. Nonetheless, some clear differences emerge from the inspection of the experimental profiles. First, all the JET discharges have standard H-mode core profiles, i.e. they do not have Internal Transport Barriers (ITB). This is not the case for the JT-60U pulses: most discharges (in particular at $q_{95} = 5.1$) show an ITB, although the channel, strength and radial position of the ITB varied depending on the heating mix (P NB or NNB + P NB) and on q_{95}. For example, figure 16 (a) shows a comparison of T_i profiles for the matching discharges 59219 (JET) and JT-60U E43072 (P NB) and E43059 (NNB). A clear break in the slope of $T_i(r)$ is visible for both P NB and NNB JT-60U pulses, absent in the JET profiles, indicating the presence of an ITB. In this example, the profiles outside the ITB radius have similar gradients in both devices. The density profiles for the same three discharges are shown in figure 16 (b): these profiles show a distinctive feature that is common to many of the JT-60U plasmas analysed in this work: the profiles (in this case of n_e, but in other examples, also T_e and/or T_i) have very flat gradients in the outer part of the plasma. Another example is shown in figure 16 (c), where $\nabla T_i(r)$ of the JT-60U plasma is much lower than for JET over the outer half of the plasma radius. The central T_i values for the two discharges are similar because of the ITB on the ion channels for $\rho < 0.5$. These observations point to differences in transport in the plasma core in the two devices (both the presence of flat gradient in the outer bulk plasma region as well as that of ITBs), that clearly affect the plasma core energy content and could possible also influence the pedestal parameters. In the particular case of the $q_{95} = 3.1$ discharges, the difference in the core density profiles is approximately sufficient to account for the lower stored energy compared to the JET case.

DISCUSSION

As described in section 1, the expectation from pedestal dimensionless identity experiments between JT-60U and JET was that the results would have provided a highly constrained but straightforward verification of the validity of the dimensionless scaling approach, given the very similar size of the two devices (resulting in dimensionless identical plasmas with very similar dimensional plasma parameters). In reality, the experiments have shown the difficulty of obtaining correctly dimensionless scaled plasma parameters in JET and JT-60U. The pedestal temperature and especially the density of the JT-60U similarity H-modes reach, in general, values below those of JET: a dimensionless match of PNB heated H-modes in JT-60U and JET could be achieved only by “downgrading” the H-mode pedestal performance of the JET similarity pulses, by operating at low power above the H-mode threshold and/or using external gas puff to reduce the pedestal pressure [14].

The discrepancy between experimental results and expectations motivates further comparative analysis of the experimental conditions on both devices, to identify other physics phenomena that

may influence the pedestal characteristics. Two main differences are identified between JET and JT-60U identity plasmas: the inverse aspect ratio, and the magnitude of the toroidal field ripple and fast ion losses.

The influence of ε (ε = 0.29 for JET and 0.25 for JT-60U) on the pedestal MHD stability is discussed in detail in [13]. The influence of ε was evaluated starting from the ideal MHD analysis (carried out with the HELENA and MISHKA codes [10], [9]) of Type I ELMy H-mode JET plasma, of the similarity series. The plasma and the walls were then moved rigidly outwards, changing ε in steps from the JET to the JT-60U value. It was found that the normalized pressure gradient α, $\propto$, ε, and therefore the reduction in the sustainable pressure gradient (and of the total pressure, assuming similar pedestal widths) by aspect ratio effects is significantly less than that observed experimentally.

A major difference between JET and JT-60U identity configuration is the B_T ripple, ~ 0.1% in JET compared to ~ 1.2% in JT-60U (low field side–separatrix value). As mentioned in section 3.1, ripple-induced fast ion losses in JT-60U are substantial, of the order of several MW for the plasmas investigated in this paper. As shown by previous works, the resulting edge electric field may provide a counter-rotation source at the plasma edge sufficient for JT-60U plasmas to counter-rotate even for net positive parallel momentum injection (figure 6). Experiments where a large fraction of perpendicular PNB were substituted by (low losses) co-NNB gave apparent conflicting results: at low q, a modest increase of the pedestal pressure was observed, in contrast to the high q plasmas, where the use of NNB resulted in a sharp change in pped and in the highest pedestal pressures for that current and field. As described in section 3.1 this different effect could be simply attributed to the fact that the reduction in the fast ion losses in the low q experiments (only ~ 35% to compare with ~ 60% at high q) was insufficient to affect significantly the plasma pedestal behaviour. In both cases, though, the plasma toroidal rotation changed in a similar way: V_{tor} becomes less negative, as shown in figure 6. The effect of toroidal field ripple and rotation was investigated in detail in JT-60U in a series of experiments carried out after those described in this work. [22] reports in detail the effect of toroidal field ripple and rotation on the H-mode pedestal in JT-60U. In these experiments, the magnitude of the ripple was changed by increasing in steps the minor radius of the plasma, therefore increasing the ripple (low field side–separatrix value) from ~ 0.4% to ~ 1.2% and finally to ~ 2%. Fast ion losses and rotation were also varied, at constant P_{in}, by carefully adjusting the beam mix. The results of this experiment indicate that toroidal field ripple directly affects the H-mode pedestal: [22] in fact report an increase of the pedestal pressure for the lowest value of ripple, and a correlation of p_{ped} with the magnitude of fast ion losses. At the same time, no strong link was found between pedestal pressure and toroidal rotation, although the range of variation of V_{Tor} was not very large. Finally, the increase of pedestal pressure at reduced ripple is found to be due to increased pedestal density, while the temperature (T_e and T_i) does not change significantly. There are strong similarities between these results and the result of this study of JET and JT-60U pedestal parameters.

A second major differences observed between JET and JT-60U H-modes is in the ELM behaviour: both ELM frequency and ELM power losses (or inter-ELM transport) are very different in the two

devices. As described in section 3.3, f_{ELM} in JT-60U is always higher (by up to 50%) than in JET, with the exception of the high q, NNB heated case. Furthermore, the prompt ELM energy loss associated to each ELM crash is much smaller in JT-60U than in JET, resulting in inter-ELM transport a factor of two higher in JT-60U then in JET, in all cases. The link between ELM frequency, losses, ripple and rotation is analysed by [5], using data from the same set of discharges studied by [22]. The author reports a clear link between the increase in the normalized ELM losses ($\Delta W_{ELM}/W_{Ped}$) and reduction of fast ion losses (as a fraction of the total input power), rather than with V_{Tor} . On the other hand, [5] also reports that f_{ELM} is directly linked to rotation, specifically that the ELM frequency decreases when V_{Tor} is less negative, independently of the magnitude of fast ion losses. This result and the different response of f_{ELM} to changes in toroidal rotation at low and high q_{95} in the JET/JT-60U similarity experiments are difficult to reconcile.

While experimental observation strongly suggests a link between toroidal field ripple and pedestal and ELM behaviour, the physics mechanism responsible linking pedestal stability and transport to toroidal field ripple is not yet known. Concentrating on the q_{95} = 5.1 results, three possible mechanisms may be put forward to qualitatively explain the improvement of the pedestal with reduced ripple losses.

The first is a possible effect of rotation on the pedestal ideal MHD stability. The pedestal MHD stability of the high p_{ped} JT-60U discharge E43075 with NNB was analysed with the MISHKA-1 code and compared to that of the same discharge in the phase with PNB only. The results of the analysis are shown in figure 17, with the four times selected for the MHD analysis indicated by vertical dashed lines in figure 7. It is found that the experimentally calculated normalized pressure gradient in the s-α diagram (“operating point”, green dot in figure 17) reaches, at most, marginal access to second stability in the PNB phase of the discharge. In contrast, the higher p_{ped} obtained with NNB corresponds to the operating point entering the second stability region, with the normalized pressure gradient in the pedestal increasing as the edge magnetic shear decreases.

For the same JT-60U discharge, the effect of plasma rotation (shear) was investigated with the MISHKA-D code [2] that includes finite gyro-radius effects of the ion diamagnetic drift on ideal MHD modes stability. It is found that, for the specific conditions analysed, imposing a negative toroidal velocity has a very small destabilizing effects compared to the results from the MISHKA-1 analysis, insufficient to explain the large difference in pedestal pressures between the PNB and NNB phase of E43075. Parametric studies of the effect of rotation on pedestal MHD stability are reported in [17], and show that toroidal shear can change the growth rate of intermediate to high *n* peeling-ballooning modes, but cannot stabilize modes with $n \lesssim 20$, that are dominant modes in Type I ELMy H-modes.

The second possible mechanism that could link the pedestal pressure and confinement to ripple is a direct effect of toroidal rotation on edge transport. Specifically, sign and magnitude of rotation at the plasma edge could change the local shear and affect shear turbulence suppression and/or the local potential profiles (neoclassical equilibrium). While the exact evaluation of these effects require

numerical turbulence analysis, an order-of-magnitude evaluation can be done on the main terms of the force balance equation, with the assumptions that the poloidal velocity is zero inside the separatrix and Scrape-Off Layer sheath conditions outside the separatrix. The shear due to toroidal velocity may influence turbulence suppression if its contribution is dominant compared to that generated by the edge gradients, while the contribution neoclassical equilibrium could be affected if the toroidal velocity contribution is of the order of the gradient terms. For typical pedestal conditions encountered in the JET/JT-60U experiments, it is found that the contribution to the shear due to the pedestal and SOL gradients is (in normalized units) ≈ 1, while that coming from toroidal rotation is ≈ $\pm 0.5 - 1\times10^{-2}$, for toroidal rotation ~ 5kHz and q_{95} varying from 5 to 3. Therefore, this evaluation would indicate that, for the typical values of V_{Tor} (or of the variation of V_{Tor}) observed in the JET/JT-60U similarity experiments, the effect on shear is too small to affect turbulence stabilization or the potential structure in the plasma edge, independently of the direction of V_{Tor}.

Finally, another hypothesis under investigation is that toroidal field ripple may have a direct effect on thermal ion transport [12], [9]. The basic idea at the root of the analysis is that even a relatively small enhancement of transport due to ripple may have a significant impact on the H-mode pedestal, due to the strong transport suppression characteristic of that region. Simulations of JET and JT-60U plasmas have been carried out with the Monte Carlo orbit-following code ASCOT, including simulations of JET plasmas with artificially enhanced ripple. The simulations show that ripple increases both diffusive and convective losses on the thermal ion population, both leading to changes in the edge plasma potential, although the magnitude of the potential change is perhaps too small to justify the increased transport. Based on the experimental observation that one of the main effect of ripple on the JT-60U pedestal seems to be an increased edge particle diffusion, [12] suggests that convective losses could be the dominant result of ripple in the H-mode pedestal. JETTO simulations with artificially increased convection can reproduce qualitatively the high ELM frequency, small ELM amplitude and reduced pedestal pressure observed experimental.

CONCLUSIONS AND OUTLOOK TO ITER

The results of the experiments described in this paper, carried out between two fusion devices of very similar size, show that the dimensionless scaling approach for the prediction of plasma performance is valid only provided that no additional physics mechanism plays an important role. In the case of the JET/JT-60U, the large ripple losses in JT-60U are the most probable candidate causing the observed discrepancies between actual and scaled (predicted) pedestal plasma performances. The physics mechanisms linking toroidal field ripple and H-mode pedestal parameters are not yet understood, although simulations of ripple-induced changes in thermal ion transport qualitatively reproduce some of the experimental observations.

The possible influence of toroidal field ripple on plasma transport may have some relevance for the performance of future ITER plasmas. In fact, ITER is equipped with only 18 toroidal field coils and, in spite of the large distance between the coils and the plasma, the toroidal field ripple in the

region of the outer midplane at the separatrix of typical ITER reference equilibria is ~ 1%. Calculations show that this value is not acceptable since it generates too high fast ion losses, and localised hot spots on plasma facing components (especially the limiters). Ferromagnetic insets are being designed (ferritic slabs to be located in the vacuum vessel interspace) to reduce the ripple magnitude. The first design of these insets reduces the value of the ripple at the separatrix at the outer midplane to ~ 0.6%, while a newer design featuring a poloidally continuos band of ferritic elements, reduces the ripple even further, down to ~ 0.3–0.4% (depending on the exact radial location of the separatrix). Fast ion losses and magnetic field line bending appear to be tolerable for both ferritic inset designs, being of the order of 1% or less of the total ± power for all full field ITER scenarios. On the other hand, although small, these values of ripple are approximately intermediate between those of JET (~ 0.1%) and JT-60U (~ 1%), and could be still significant for pedestal transport and ELMs parameters. The present level of understanding of the effects of ripple on transport (magnitude, plasma volume affected, etc.) does not allow a firm prediction to be made for ITER at this point in time. The possible consequences for ITER may be different depending on the underlying physics mechanism responsible for the pedestal degradation and changes in the ELM characteristics observed in the experiments in JT-60U described in this paper.

The analysis presented in this work has not found a convincing explanation to link differences in toroidal rotation between JET and JT-60U to the difference pedestal and ELM characteristrics in the two devices. The calculated V_{Tor} for the ITER Q = 10 reference scenario (ASTRA transport simulations, no ripple effects included) is rather small but positive, across the whole plasma radius. Since the predicted fast ion ripple induced losses in this ITER scenario are very small, they will not significantly affect plasma toroidal rotation and therefore should not affect the ITER pedestal parameters. The evaluation of the effect of low V_{Tor} in ITER, significantly lower than normally obtained in present-day tokamaks, in terms of impact on the edge transport barrier is outside the scope of this paper .

Since the time of the experiments described in this work, JT-60U has installed a number of ferromagnetic tiles, achieving a reduction of the average ripple magnitude by ~ 2 for B_T ~ 1.8T. First results of new experiments in JT-60U [11] seems to confirm a strong effect of ripple on ELM frequency and losses. Finally, an experimental investigation of the effects of B_T ripple on H-mode pedestal and plasma performance will take place in the coming experimental campaign of JET, in collaboration with JAEA. The experiments will take advantage of the ability in JET of changing the ripple in a controlled way from ~ 0.1% to ~ 2% by controlling the differential current between odd and even numbered toroidal field coils, and therefore to reproduce both the JT-60U and ITER ripple values on the same device. The resulting ripple topology of JET will be very similar to that expected in ITER with ferromagnetic insets, including the very small ripple magnitude in the x-point region. For the same ripple magnitude, NB fast ion losses are expected to be much lower in JET than in JT-60U, especialy when compared to perpendicular beams in JT-60U. This difference may allow to separate out experimentally fast ion losses effects and direct ripple effects on the pedestal and ELMs.

ACKNOWLEDGEMENTS

The authors thank the EFDA-JET and JT-60U teams and collaborators for help and support in the execution and analysis of the joint experiments presented in this paper. On author (G Saibene) thanks Y Gribov and A Polevoi of the ITER Team for the ASTRA simulations and M Roccella (LT-Calcoli, Italy) for calculations of ITER ripple values. G Saibene also thanks Drs. A Peters and B Scott (IPP, Garching) for their help in the evaluation of rotational effects on pedestal transport. Finally, these experiments have been carried out under the patronage of the ITPA, and in the framework of the IEA/LTA international agreement.

REFERENCES

[1]. Challis, C.D. and the JET Team (1995). Fus Eng Design **26**, 17.

[2]. Huysmans, G.T.A., Sharapov, S.E., Mikhailovskii, A.B., and Kerner, W. (2001). Phys of Plasmas **8**, 4292.

[3]. ITER Physics Basis (1999). Nuclear Fusion **39**, 2175. by the ITER Physics Expert Groups on Confinement and Transport and Confinement and Modelling and Database.

[4]. Kamada, Y., Yoshino, R., Ushigusa, K., et al. (1996). Fusion Energy 1996 1, 247. IAEA-CN-64/A1-6.

[5]. Kamiya, K., Urano, H., Koide, Y., et al. (2006). Plasma Phys Control Fus **48**, A131.

[6]. Koide, Y., Tuda, T., Ushigusa, K., et al. (1992). Plasma Phys Control Nucl Fus Res 1992 **1**, 777. IAEA-CN-56/E-3-1.

[7]. Kuriyama, M., Akino, N., Ebisawa, E., et al. (2002). Fus Science Technol **42**, 424.

[8]. Lonnroth, J., Parail, V., Johnson, T., et al. (2006). Modelling of Effects of Ripple-Induced Thermal Ion Losses on JET and JT-60U H-Mode Plasmas. Proc 33th Conf on Plasma Physics, Rome (I) - paper P1.080.

[9]. Lonnroth, J.-S., Parail, V.V., Corrigan, G., et al. (2003). Plasma Phys Control Fus **45**, 1689.

[10]. Mikhailovskii, A. B., Huysmans, G.T.A., Kerner, W.O.K., and Sharapov, S.E. (1997). Plasma Phy Rep **23**, 844.

[11]. Oyama, N., Urano, H., Yoshida, M., et al. (2006). Enhanced ELMy H-Mode Performance with Reduced Toroidal Field Ripple in JT-60U. Proc 33rd Conf on Plasma Physics, Rome (I) - paper O2.001.

[12]. Parail, V., Evans, T., Johnson, T., et al. (2006). Theoretical Analysis and Rpedictive Modelling of ELMs Mitigation by Enhanced Toroidal Ripple and Ergodic Magnetic Field. to be presented at the 21st Fus Energy Conf - Chendu, China, October 2006.

[13]. Saibene, G., Hatae, T., Campbell, D.J., et al. (2004). Plasma Phys Control Fusion **46**, A195.

[14]. Saibene, G., Horton, L. D., Sartori, R., et al. (1999). Nuclear Fusion **39**, 1133.

[15]. Saibene, G., Lomas, P.J., Becoulet, M., et al. (2001). The Effect of Plasma Shape on Density and Confinement of ELMy H-Modes in JET. Proc 28th Conf on Controlled Fusion and Plasma Physics, Madeira (PT) - paper P3.002/Or.28.

[16]. Sartori, R., Lomas, P., Saibene, G., et al. Scaling Study of ELMy HMode Global and Pedestal Confinement at High Triangularity in JET. IAEA, Vienna. Proc of the 20th Fusion Energy Conf 2004, November 2004, paper IAEA-CN-116/EX/6-3 and http://wwwnaweb. iaea.org/napc/physics/fec/fec2004/datasets/index.html.
[17]. Snyder, P.A., Burrel, K.H., Wilson, H., et al. (2006). Stability and Dynamics of the Edge Pedestal in the Low Collisionality Regime: Physics Mechanisms for Steady-State ELM-Free Operation. 21st International Conference on Plasma Physics and Controlled Nuclear Fusion Research 2006, Chengdu, China (IAEA Vienna), Paper TH/4-1Ra.
[18]. Takizuka, T. F. A., Tsuchida, K., et al. (2000). Plasma Phys Control Fus **42**, A289.
[19]. Tani, K., Azumi, M., and Kishimoto, H. (1981). J. Phys. Soc. Jpn. 50, 1726.
[20]. Tobita, K., Tani, K., Kusama, Y., et al. (1995). Nucl Fusion **35**, 1585.
[21]. Urano, H., Kamada, Y., Shirai, H., et al. (2002). Plasma Phys Control Fus **44**, A473.
[22]. Urano, H., Kamiya, K., Koide, Y., et al. (2006). Plasma Phys Control Fusion **48**, A193.

	JET	**JT-60U**
R (m)	2.97	3.43
a (m)	0.86	0.87
ε	0.26	0.25
κ	1.48	1.45
δ	0.27	0.28

Table 1: Main geometrical parameters of the equilibria used in the experiment (see figure 1)

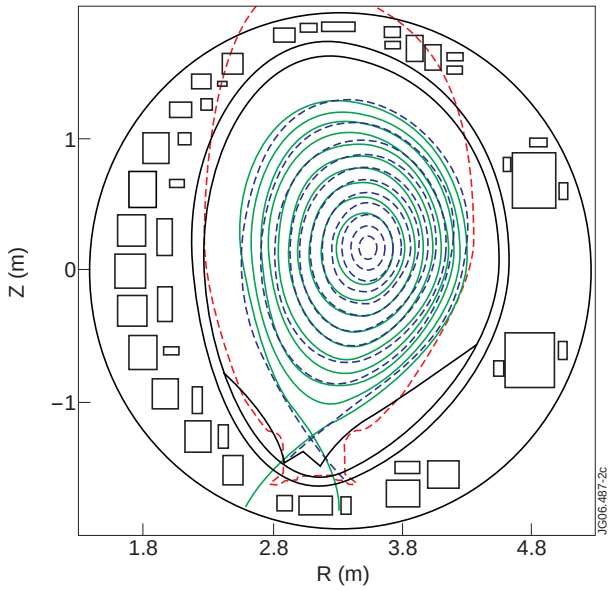

Figure 1: Equilibrium reconstruction for a plasma discharge in JT-60U (green continuous line, pulse E41386, I_p = 1.8MA – B_T = 3.1T) and one in JET (blue dashed line, pulse 59215, I_p = 1.9MA – B_T = 2.9T, shifted radially by ≈ +0.46m). The dashed contour represents the profile of the interior of the JET vacuum vessel, while the full black line vessel contours and poloidal field coils are those of JT-60U.

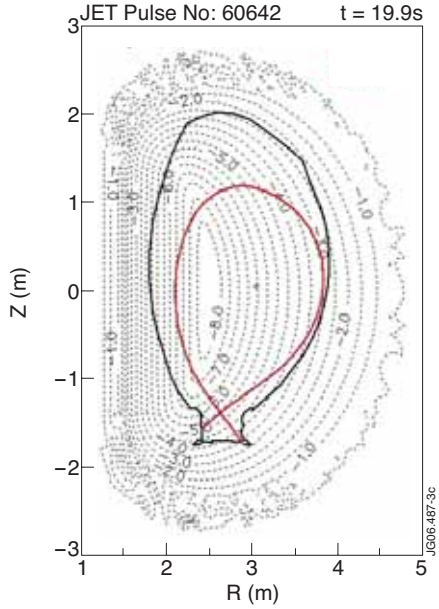

Figure 2: TF ripple map for JET, with 32 coils all carrying the same current (standard TF operation). The dotted lines identify surfaces of equal ripple amplitude, in logarithmic scale. The equilibrium used for the similarity experiments is shown in red.

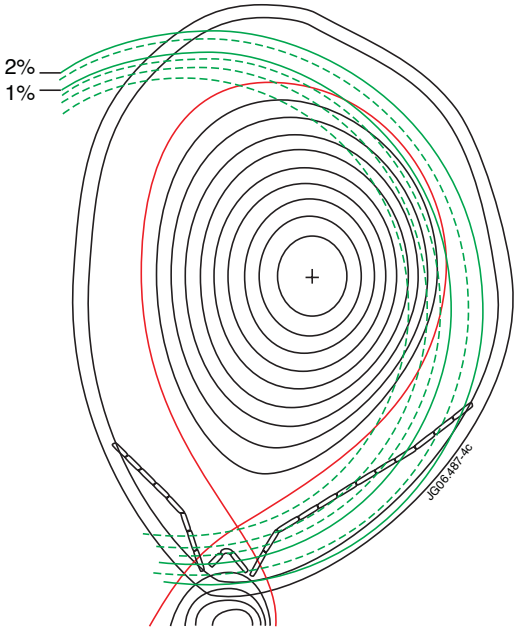

Figure 3: TF ripple map for JT-60U of the equilibrium used for the JET similarity experiments. Surfaces of equal ripple intensity (in %), relevant for the estimation of the ripple intensity in the pedestal region are shown.

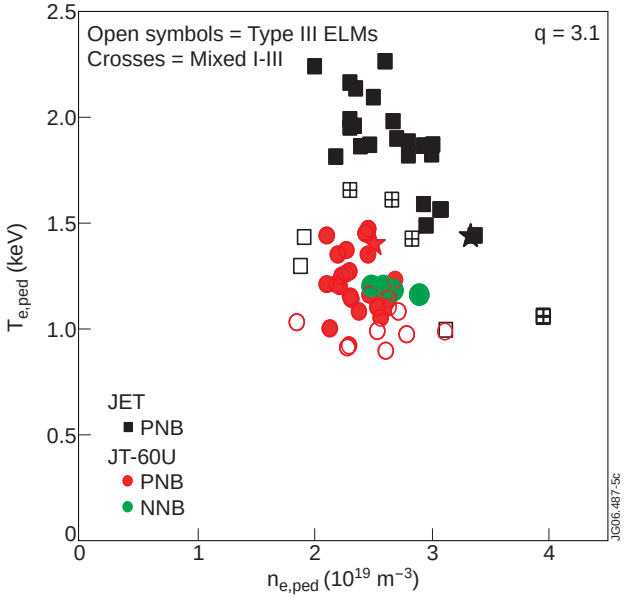

Figure 4: Comparison of JET and JT-60U pedestal T_e versus n_e (top of the pedestal values), for all similarity discharges at q_{95} = 3.1. The black squares are for JET data, the dots for JT-60U data: red with PNB injection and green with NNB injection. The stars mark the pedestal values corresponding to the best dimensionless matching points.

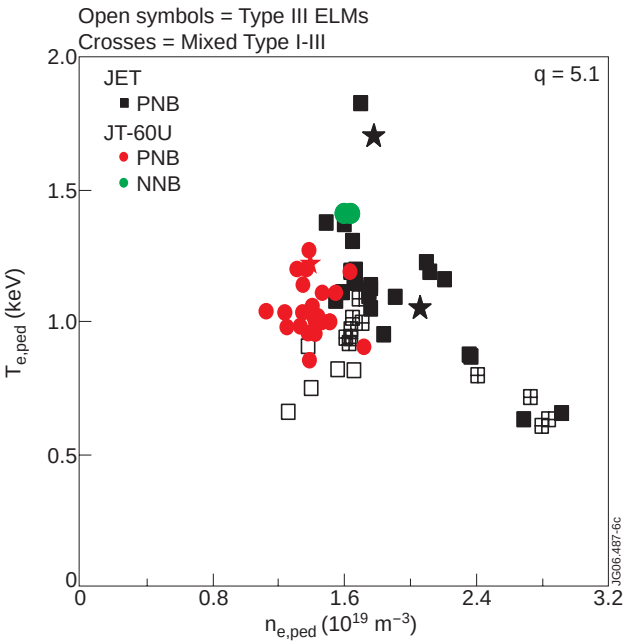

Figure 5: Comparison of JET and JT-60U pedestal T_e versus n_e (top of the pedestal values), for all similarity discharges at q_{95} = 5.1. The symbols are the same as in figure 4.

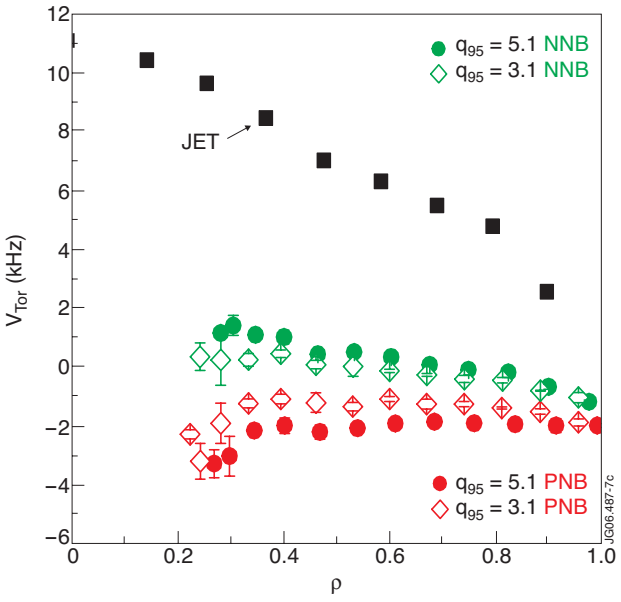

Figure 6: Typical toroidal rotation profiles ($V_{Tor,}$ kHz) for JET and JT-60U plasmas. Black squares: JET pulse 59219 (1.8MA/2.9T). From JT-60U, 4 profiles are shown. Two are from pulse E43058 (1.8MA/3.1T): open red lozenges, PNB only, open green lozenges, PNB + NNB; the other two are from pulse E43075 (1.08MA/3.1T): full red dots, PNB only, open green dots, PNB + NNB. For both pairs of JT-60U pulses, the total net input power is approximately constant (within ~10%), independently of the beam mix.

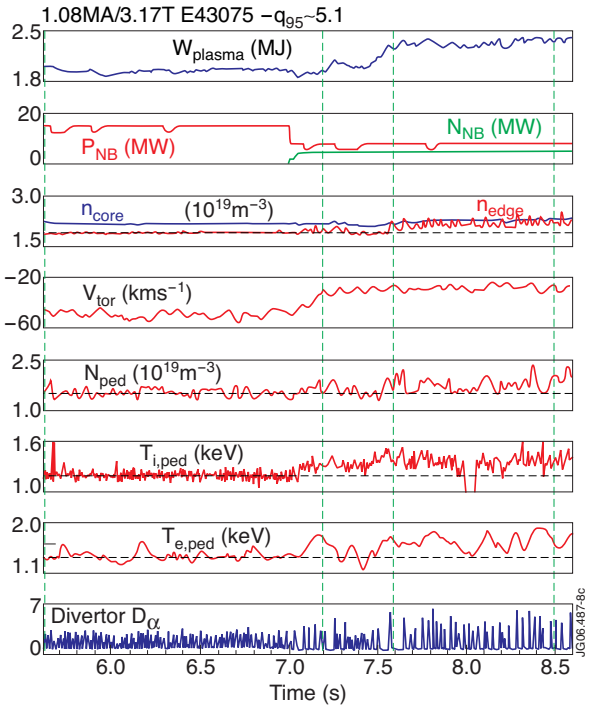

Figure 7: Selection of time traces from JT-60U pulse E43075 (1.08MA/3.17T , q_{95} = 5.1). From top to bottom: Total plasma stored energy W (MW); total neutral beam injected power (PNB, red line; NNB green line, MW); plasma average electron density in the (ncore, blue line) and near the top of the pedestal (nedge, red) in 10^{19} m^{-3}; edge toroidal velocity (V_{tor}, kms"1); top-of-the pedestal density (nped, 1019m"3); top-of-thepedestal ion temperature (Ti,ped, keV) and electron temperature ($T_{e,ped}$, keV) and, last box, divertor Hα emission, in a.u.. The dotted line at t = 7s marks the point where perpendicular PNB sources are switched off and replaced by NNB sources, keeping the net input power approximately constant. The 4 green dashed lines mark the times of MHD stability analysis (see section 4).

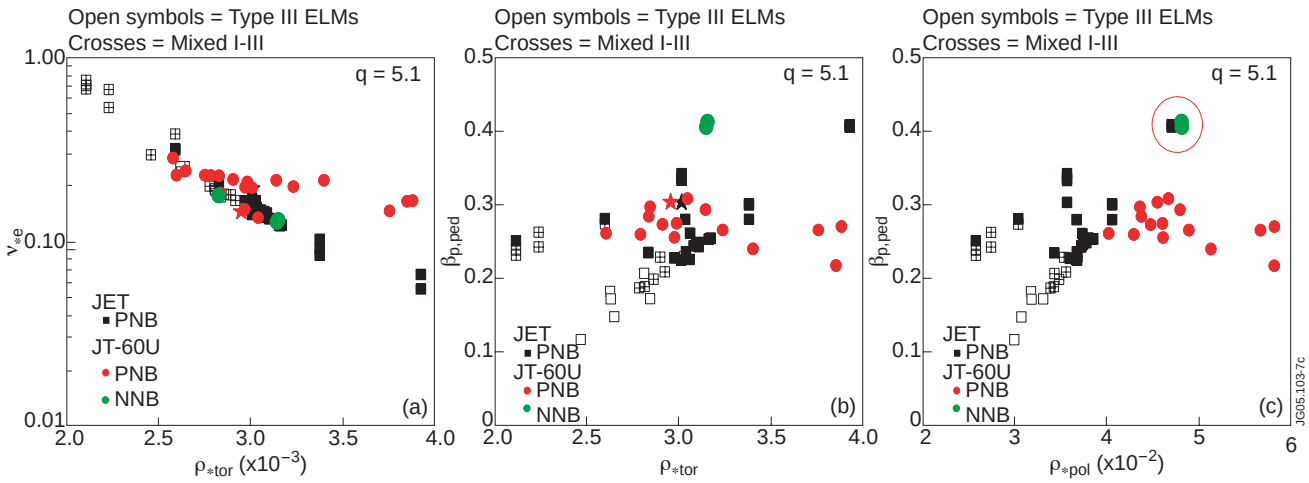

Figure 8: Dimensionless pedestal parameters for q_{95} = 5.1 data in JET and JT-60U. (a) ρ^*_{tor} versus ρ^*_e, (b) $\beta_{p,ped}$ versus ρ^*_{tor} and (c) $\beta_{p,ped}$ versus ρ^*_{pol}. The best matching discharges with PNB heating for both devices are marked with a star.

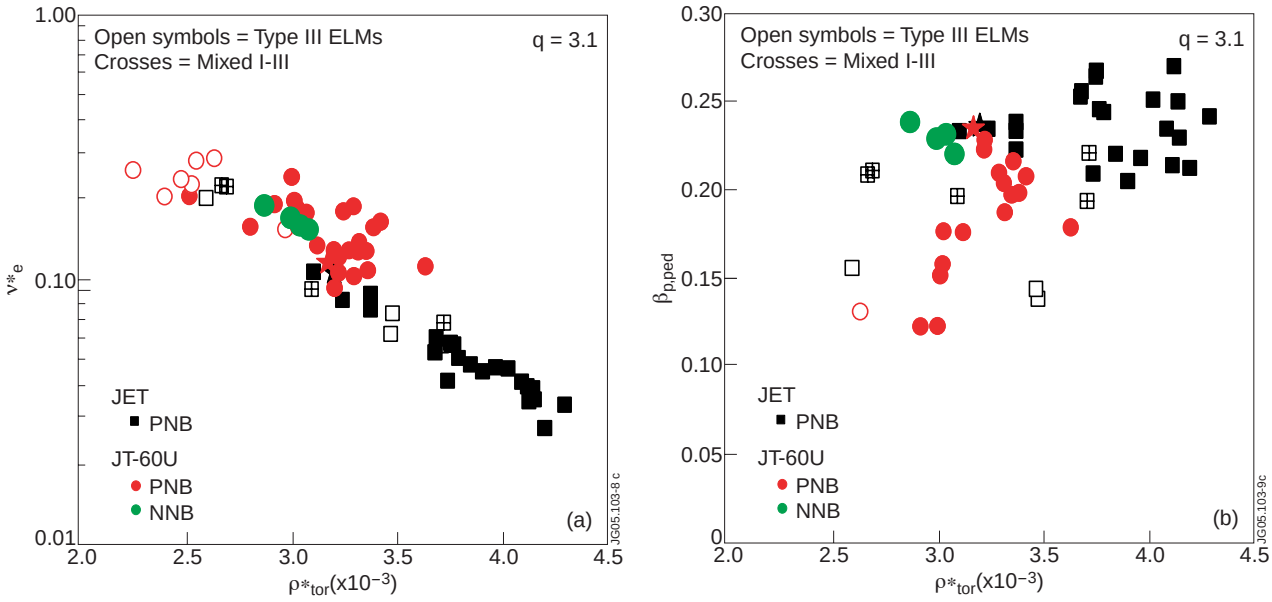

Figure 9: Dimensionless pedestal parameters for q_{95} = 3.1 data in JET and JT-60U. (a) ρ^*_{tor} versus ν^*_e and (b) $\beta_{p,ped}$ versus ρ^*_{tor}. The best matching discharges with PNB heating for both devices are marked with a star.

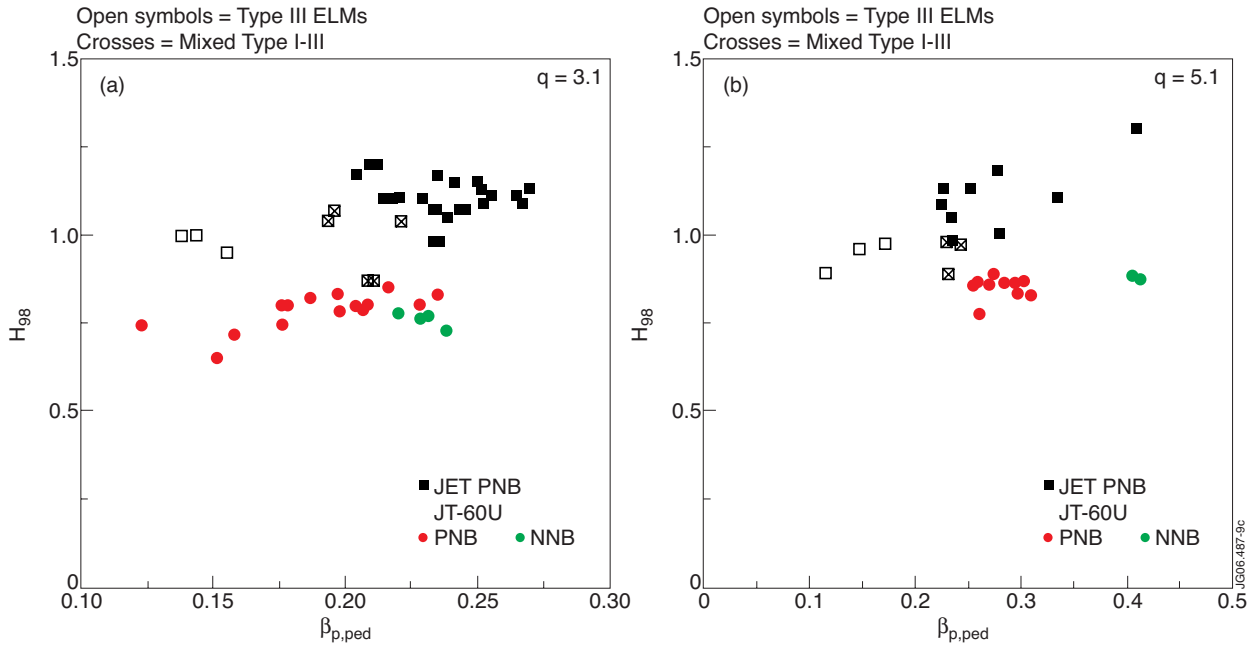

Figure 10: Thermal confinement enhancement factor H_{98} as function of $\beta_{p,ped}$ for the full data set of similarity experiments analysed in this paper. (a), shows all discharges with q_{95} = 3.1, while (b) shows all discharges with q_{95} = 5.1.

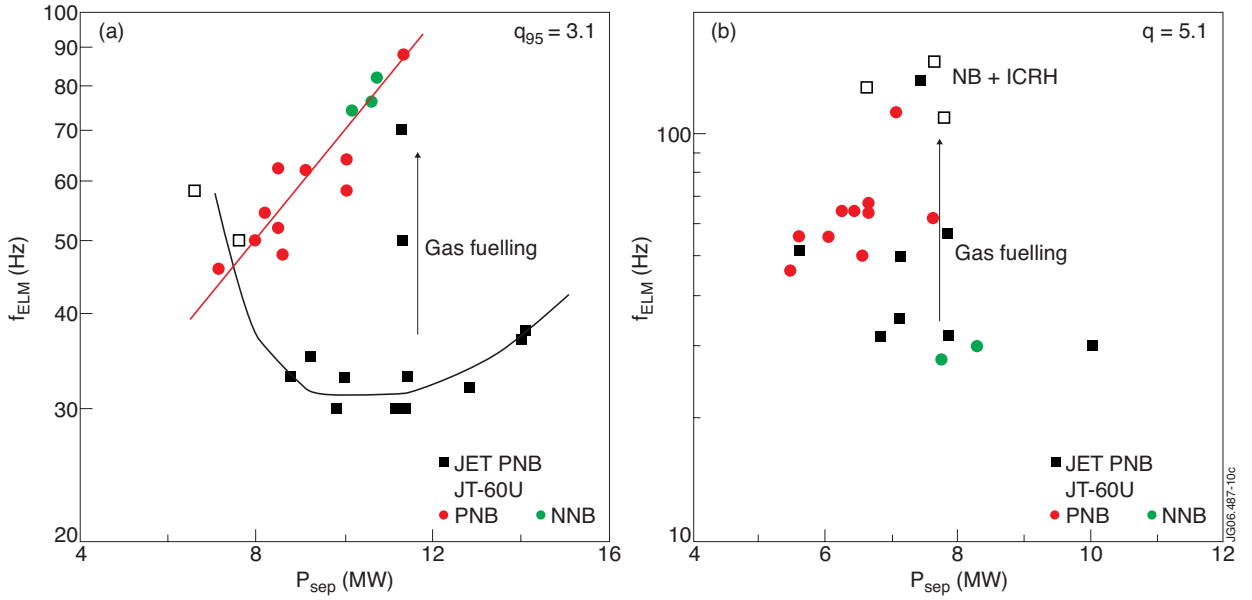

Figure 11: ELM frequency fELM as function of power across the separatrix, P_{sep}. (a): data points for q_{95} = 3.1 and (b), data points for q_{95} = 5.1. All the data points are taken at constant P_{in}. The black squares are for JET data (open = Type III ELMs, full = Type I ELMs) while the dots represent JT-60U data (red = PNB and green = NNB), Type I ELMs only.

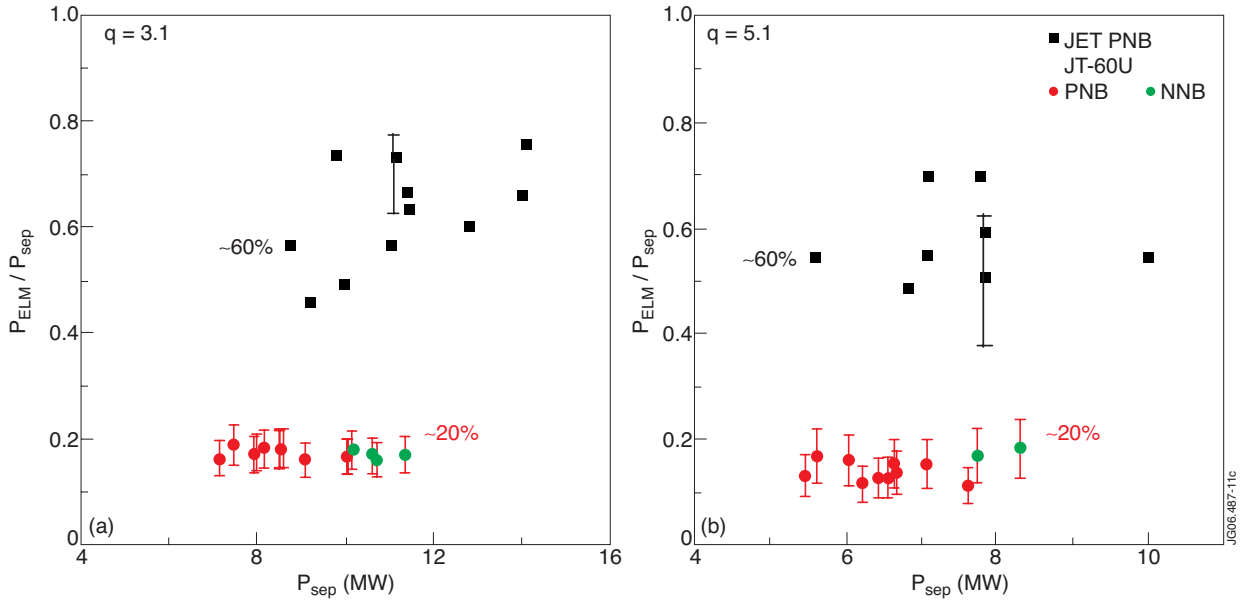

Figure 12: Fraction of loss power carried by ELMs (P_{ELM}/P_{sep}) as function of the power crossing the separatrix, for low (a) and high q_{95} (b) similarity experiments. Same symbols as in figure 11.

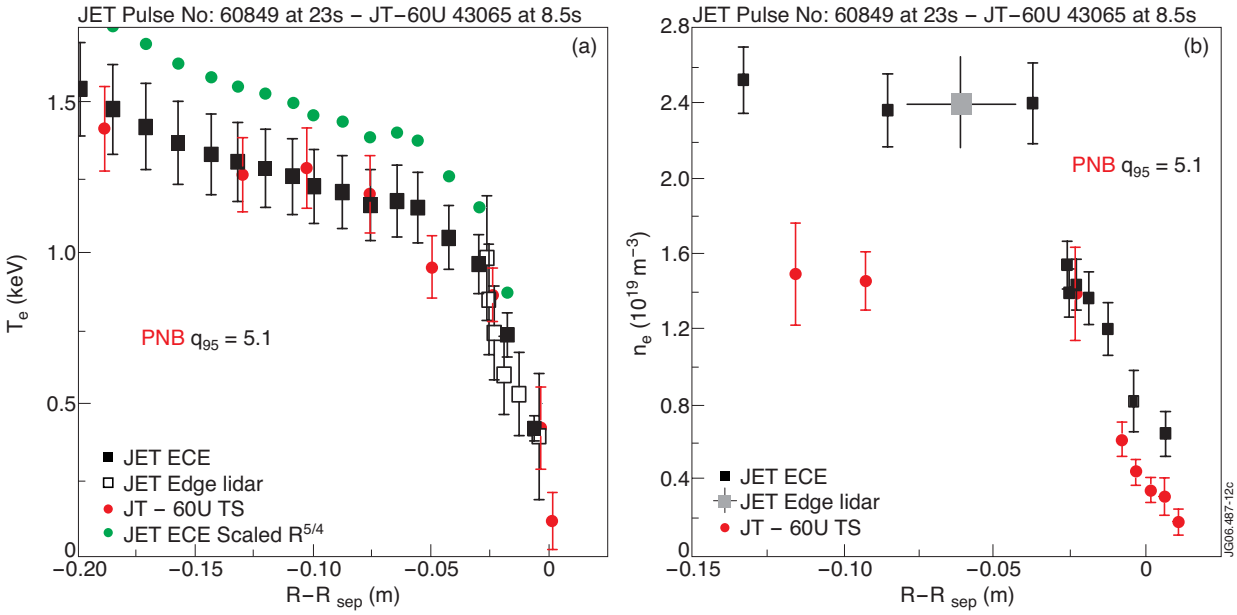

Figure 13: Left, (a) electron temperature profiles Te for the pair of dimensionless matching discharges with q_{95} = 5.1: JET Pulse No:60843 and JT-60U E43065 (PNB only) and, right, (b) electron density profiles n_e for the same pair of discharges and time slices. The profiles are plotted in real space as function of the distance from the separatrix, R – R_{sep}. Panel (a) also shows the JET T_e profile scaled to JT-60U ($\propto R^{5/4}$, pale gray symbols), for easier comparison.

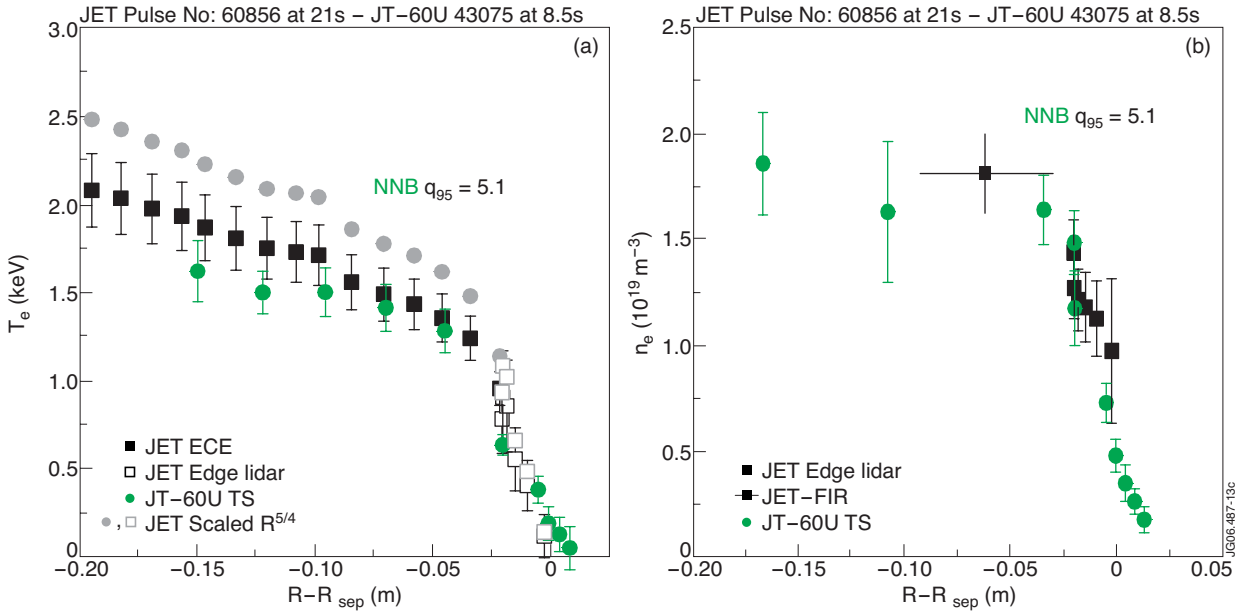

Figure 14: Left, (a) electron temperature profiles Te for the pair of dimensionless matching discharges with q_{95} = 5.1: JET Pulse No: 60856 and JT-60U E43075 (PNB+NNB) and, on the right, (b) electron density profiles n_e for the same pair of discharges and time slices. The profiles are plotted in real space as function of the distance from the separatrix, $R - R_{sep}$. Panel (a) also shows the JET T_e profile scaled to JT-60U ($\propto R^{5/4}$, pale gray symbols), for easier comparison.

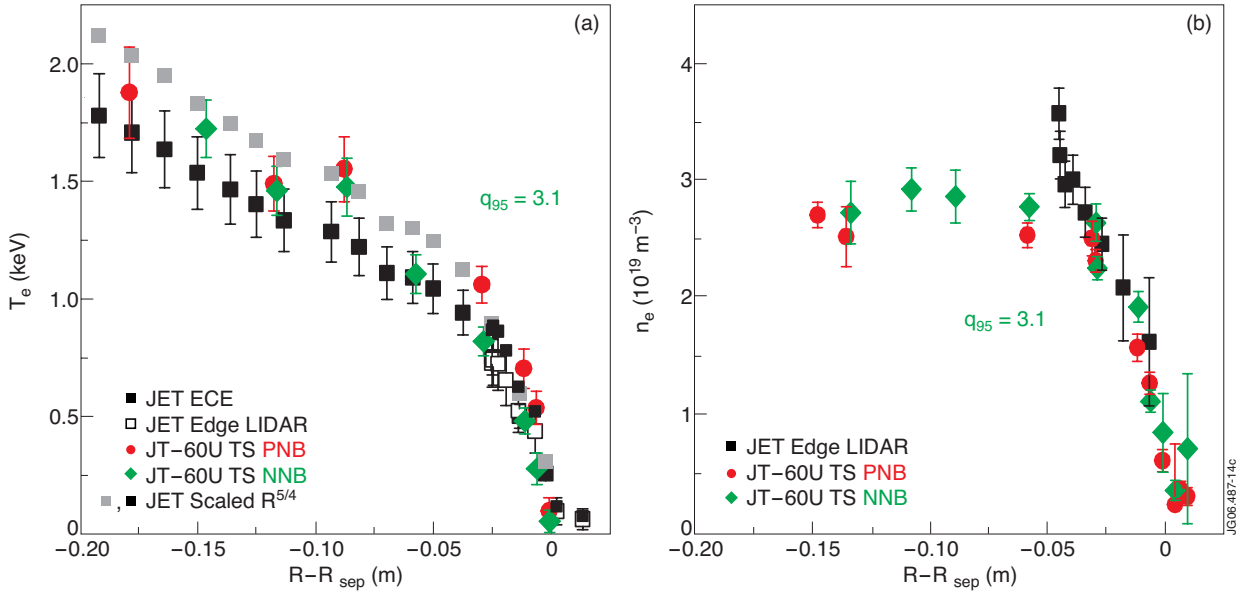

Figure 15: Left, (a) electron temperature profiles T_e for three dimensionless matching discharges with q_{95} = 3.1: JET Pulse No: 59219 and JT-60U E43072 (PNB only, red dots) and E43059 (PNB +NNB, green lozenges) and, on the right, (b) electron density profiles ne for the same pair of discharges and time slices. The profiles are plotted in real space as function of the distance from the separatrix, $R - R_{sep}$. Panel (a) also shows the JET T_e profile scaled to JT-60U ($\propto R^{5/4}$, pale gray symbols), for easier comparison.

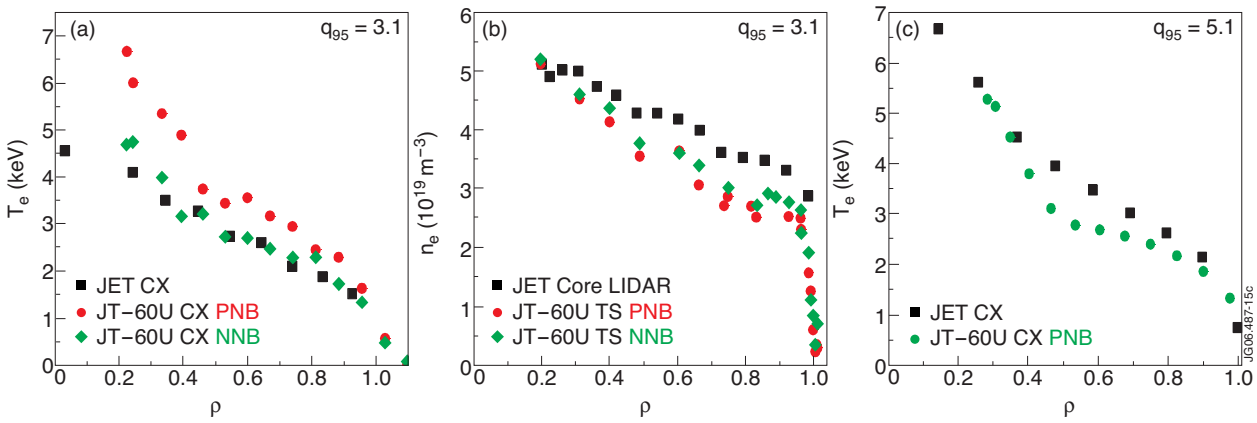

Figure 16: Comparison of some core plasma profiles for a selection of pairs of JET/JT-60U dimensionless matched plasmas (at the pedestal top). (a) and (b): Ion temperature profiles and electron density profiles as function of normalised radius ρ = r/a for the same three plasma discharges of figure 15; (c) ion temperature profiles for the matching pair of JET and JT-60U NNB injection plasmas at q_{95} = 5.1 (see figure 14)

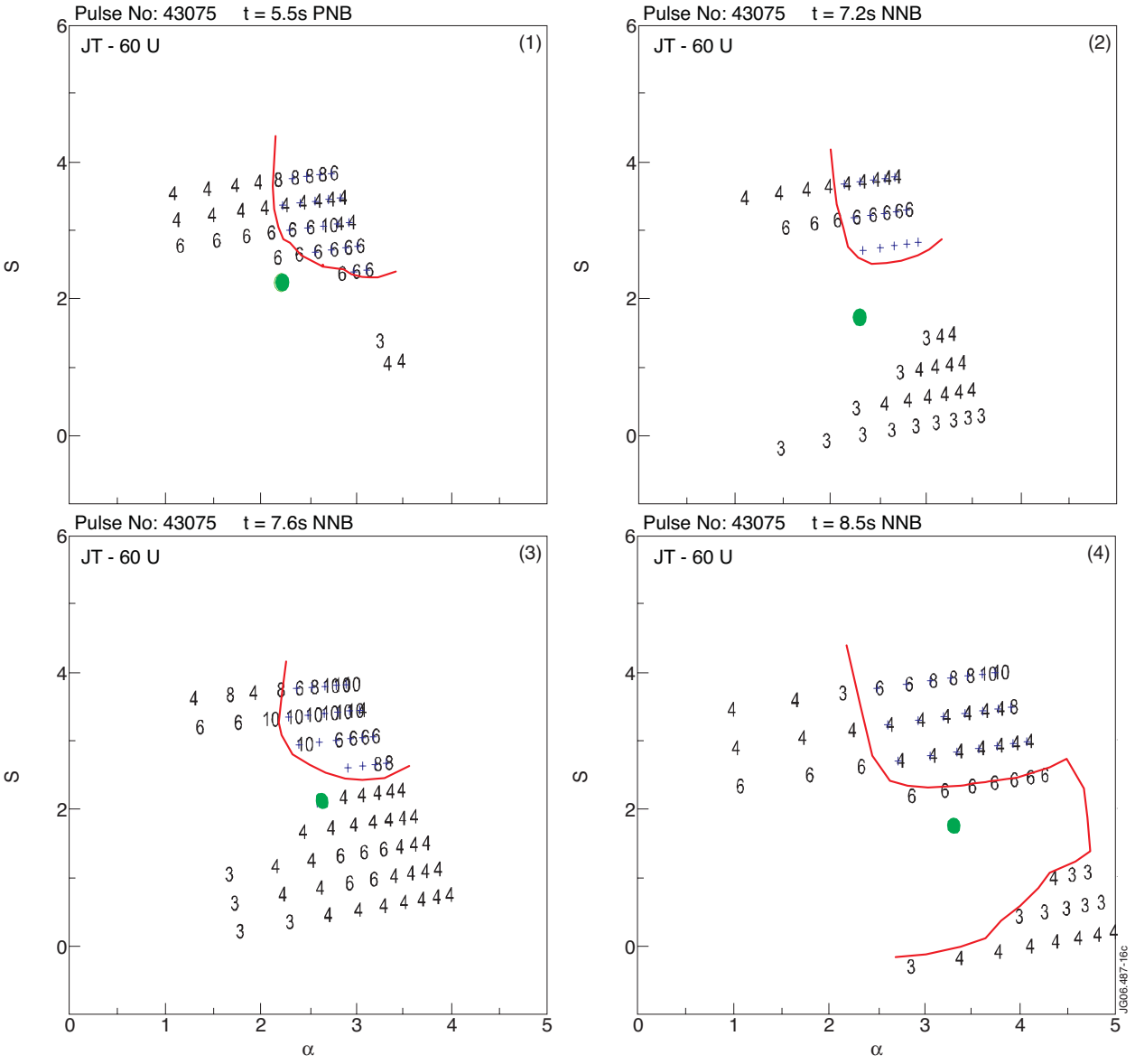

Figure 17: s−α diagram calculated for four time slices in the JT-60U discharge E43075 (see figure 7). The experimental point for each time slice is represented by the green dot; the red line shows the stability boundary for each case.